Available online at www.sciencedirect.com

ScienceDirect

journal homepage: www.elsevier.com/locate/he

$C_{60}Co_n$ complexes as hydrogen adsorbing materials

Estefanía Germán [a,*], *Julio A. Alonso* [a], *Ewald Janssens* [b], *María J. López* [a]

[a] *Department of Theoretical, Atomic and Optical Physics, University of Valladolid, 47011 Valladolid, Spain*
[b] *Quantum Solid-State Physics, Department of Physics and Astronomy, KU Leuven, 3001 Leuven, Belgium*

HIGHLIGHTS

- Adsorption of H_2 on neutral $C_{60}Co_n$ complexes has been studied by DFT calculations.
- The Co atoms form compact clusters on the surface of C_{60}.
- Dissociative chemisorption of H_2 on $C_{60}Co_n$ is energetically more stable than molecular adsorption.
- Activation barriers for H_2 dissociation depend on size and charge of the $C_{60}Co_n$ complexes.

GRAPHICAL ABSTRACT

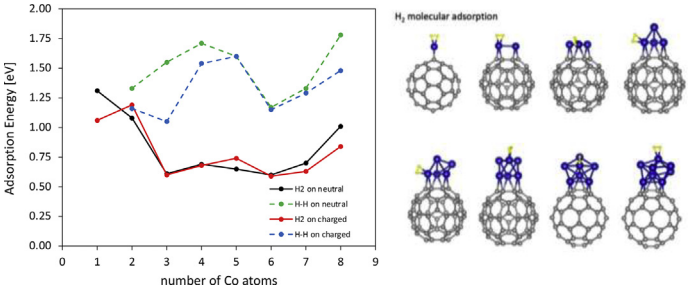

ARTICLE INFO

Article history:
Received 25 December 2020
Received in revised form
19 March 2021
Accepted 20 March 2021
Available online 15 April 2021

Keywords:
Density functional theory
Hydrogen
fullerene
Cobalt
Energy storage

ABSTRACT

An active line of contemporary research is dedicated to the adsorption and storage of hydrogen on metal-doped carbon materials. Using density functional theory and van der Waals corrections we have studied molecular and dissociative adsorption of H_2 on neutral and cationic $C_{60}Co_n$ complexes with n = 1–8. The Co atoms form compact clusters on the surface of the fullerene. Dissociative chemisorption of one H_2 molecule is more stable than molecular adsorption on neutral $C_{60}Co_n$, with the only exception of $C_{60}Co$. When $C_{60}Co_n$ is ionized, the electronic charge deficit remains localized in the cobalt cluster. The molecular and dissociative adsorption features on cationic $C_{60}Co_n^+$ and neutral $C_{60}Co_n$ complexes are in general similar, but some differences can be highlighted. Molecular and dissociative H_2 adsorption on $C_{60}Co_2^+$ are competitive; in fact, molecular adsorption is slightly more stable as a result of the localized electronic charge deficit on the Co dimer. Another difference is that the dissociative adsorption energies on some of the neutral $C_{60}Co_n$ complexes are substantially larger than the dissociative adsorption energies on the corresponding $C_{60}Co_n^+$ cationic complexes by amounts between 0.2 and 0.5 eV. Activation barriers for dissociation of the adsorbed H_2 molecule strongly depend on the charge state and cluster size. These barriers help to interpret the adsorption state (molecular or dissociated) of experimentally produced hydrogenated $C_{60}Co_n^+$ complexes. Hydrogen saturation has been studied in two

* *Corresponding author.*
E-mail address: estefania.german@uva.es (E. Germán).
https://doi.org/10.1016/j.ijhydene.2021.03.179

cases. $C_{60}Co$ adsorbs three H_2 units in molecular form, and $C_{60}Co_n$ adsorbs up to thirteen H_2 units, four dissociated and nine in molecular form.

Introduction

Hydrogen is a firm candidate to replace gasoline for cars in the near future [1]. The engine technology is advancing well: the engine is a fuel cell where hydrogen reacts with atmospheric oxygen producing an electric current that is used to drive the vehicle. Water vapor is the only waste product in the process. A key issue is the storing of hydrogen on board. The current available technology of storing hydrogen as a compressed gas at high pressures is not fully satisfactory, and a present line of intensive research is dedicated to develop efficient hydrogen storing materials [2]. A variety of these materials has been investigated. An interesting group has been termed sorbent materials [2,3]. These include, among others, carbon nanotubes [4–6], boron nitride nanotubes [7,8], inorganic and organic fullerenes [9,10], graphene nanoflakes [11,12], porous carbons [13–19], mesoporous silica [3], metal-organic frameworks (MOFs) [19], covalent-organic frameworks (COFs) [20], and clathrates [21]. In these, hydrogen is bound to the substrate by physisorption forces [22,23], so the systems are good hydrogen adsorbers only at low temperature. The bonding strength is optimized in nanostructured materials, like nanoporous carbons [15,18,24], because the confining geometry of the nanopores maximizes the interaction between hydrogen molecules and the nanopore walls [16,17].

A recent explored route to increase the amount of stored hydrogen consists in doping the materials with metal atoms or nanoparticles, and promising results have been obtained for porous carbons [25,26]. Some theoretical studies of hydrogen adsorption on carbon fullerenes doped with transition and non-transition metal atoms and clusters have been performed [27–32], and recently the reactivity of alkali metal- and transition metal-fullerene complexes towards hydrogen has been studied by a combination of experimental and theoretical work [33,34]. The experimental work was based on mass spectrometry, and this means that the hydrogenated metal-fullerene complexes are actually charged, cationic complexes. For this reason, the theoretical calculations were also performed for cationic hydrogenated metal-fullerene complexes. If hydrogenated metal-fullerene complexes are contemplated as possible sorbent materials for hydrogen storage, those systems should, evidently, be electrically neutral, to allow for massive assembling. This motivates us to perform theoretical density functional (DFT) calculations for neutral cobalt-fullerene complexes $C_{60}Co_n$ ($n = 1–8$), and to compare the results with those for the cationic complexes $C_{60}Co_n^+$. In this way, apart from treating the neutral complexes, potentially suitable for applications, we also draw information of the effect the charge state has on the reactivity with hydrogen. In addition, this study can enlighten the general problem of the interaction of hydrogen with metal-doped carbon nanostructures, because the convex curvature of the fullerene surface is also found in carbon nanotubes and may occur in the walls of porous carbons. In Section Theoretical model, a brief account of the theoretical model is given. A study of the neutral and charged $C_{60}Co_n$ complexes is reported in Section Neutral and charged C60Con complexes, and the study of molecular and dissociative hydrogen adsorption in Section Molecular and dissociative adsorption of hydrogen. Section Saturation with hydrogen gives the conclusions.

Theoretical model

Structural and electronic properties have been studied by performing DFT calculations using version 6.2.1 of the quantum-ESPRESSO suite of electronic structure codes [35]. In order to account for the electron-ion core interaction, the projector augmented wave method, known as PAW, was used, namely, C.pbe-n-kjpaw_psl.0.1.UPF for carbon and Co.pbe-spn-kjpaw_psl.0.3.1.UPF for cobalt, which amount for 4 and 17 external electrons respectively. These pseudopotentials, available from the Quantum ESPRESSO Web site [36], correspond to the following electronic configurations: $2s^2\ 2p^2$ for C, and $3s^2\ 4s^2\ 3p^6\ 3d^7$ for Co. The Perdew-Burke-Ernzerhof (PBE) functional was employed for electronic exchange and correlation [37,38]. To expand the Kohn-Sham orbitals in plane waves, a cutoff energy of 40 Ry was used, and a cutoff of 350 Ry for the charge density. The $C_{60}Co_n$ bare systems and those with H_2 adsorbed were modeled inside a cubic supercell of 17 x 17×17 Å^3; using this supercell size assures that no interaction occurs between periodic images. The gamma point for the Brillouin zone integration was used in the calculation. The Grimme-D3 [39] method was taken to account for the dispersion correction to the density functionals.

The Makov-Payne correction was applied to the charged systems [40]. This correction is used to calculate the total energy of an isolated charged system – a molecule or a cluster in a 3D supercell – with periodic boundary conditions. This method also provides an estimate of the vacuum level, so that eigenvalues can be properly aligned. The nudged elastic band (NEB) method [41,42] was employed to calculate the energy barriers and reaction pathways for the dissociation of the H_2 molecule on charged and neutral Co_nC_{60} complexes.

Neutral and charged $C_{60}Co_n$ complexes

The formation of $C_{60}Co_n$ complexes can occur in two different ways, depending on the type of experiment. The preformed Co_n cluster can be deposited on the fullerene, or the Co atoms can be deposited one by one. Therefore, in the search of low energy structures of $C_{60}Co_n$ complexes we have mimicked both

pathways; that is, we have generated initial configurations in two ways: 1) by depositing a preformed Co_n cluster on different positions on the fullerene surface, and 2) by adding one single Co atom on various positions of a preformed $C_{60}Co_{n-1}$ complex, including positions on the C_{60} surface, so not in initial contact with the Co_{n-1}. The lowest energy structures obtained for free Co_n clusters are as follows: Co_3 is a triangle, Co_4 is a tetrahedron, Co_5 is a square pyramid, Co_6 is an octahedron, Co_7 is a face-capped octahedron, and Co_8 is a bi-capped octahedron. These results are in good agreement with previous studies [43–45]. As discussed by Ma et al. [45], Co_5 has two competing isomers with similar energy, the square pyramid and a trigonal bipyramid, and different studies predict one or the other as the lowest energy structure (a small distortion of the first structure leads to the second). In our calculations the square pyramid is 0.1 eV more stable that the trigonal bipyramid.

The lowest energy structures of the neutral $C_{60}Co_n$ clusters, n = 1–8, are shown in Fig. 1. The Co atoms form clusters on top of a carbon hexagon of the fullerene. The number of Co atoms in direct contact with the fullerene is one in $C_{60}Co$, two in $C_{60}Co_2$, and three in the $C_{60}Co_3$ to $C_{60}Co_8$ cases. Co atoms in direct contact with the fullerene adopt bridge positions between neighbor C atoms, and for n = 3 to 8 form a triangular face parallel to the underlying hexagon of carbon atoms. In $C_{60}Co$, the Co bridge on top of a C-C bond common to two adjacent hexagons is 0.385 eV more stable than the Co bridge on top of a C-C bond common to a pentagon and a hexagon. The structures of the adsorbed Co clusters do not change compared to the free clusters, with two exceptions. Adsorbed Co_5 adopts the form of a trigonal bipyramid, which as mentioned is a low-lying isomer of free Co_5. And Co_7 has a pentagonal bipyramid structure on C_{60}: this is also the first low-lying isomer of free Co_7. The lowest energy structures of $C_{60}Co_n$ tend to maximize the number of Co atoms in direct contact with the fullerene surface but without subjecting the Co_n cluster to large deformations. Configurations of $C_{60}Co_2$, $C_{60}Co_3$ and $C_{60}Co_4$ with respectively one, two and two Co atoms in contact with the fullerene, are 0.4, 0.14 and 0.68 eV less stable than the corresponding lowest energy structures with one more Co atom in direct contact with the fullerene

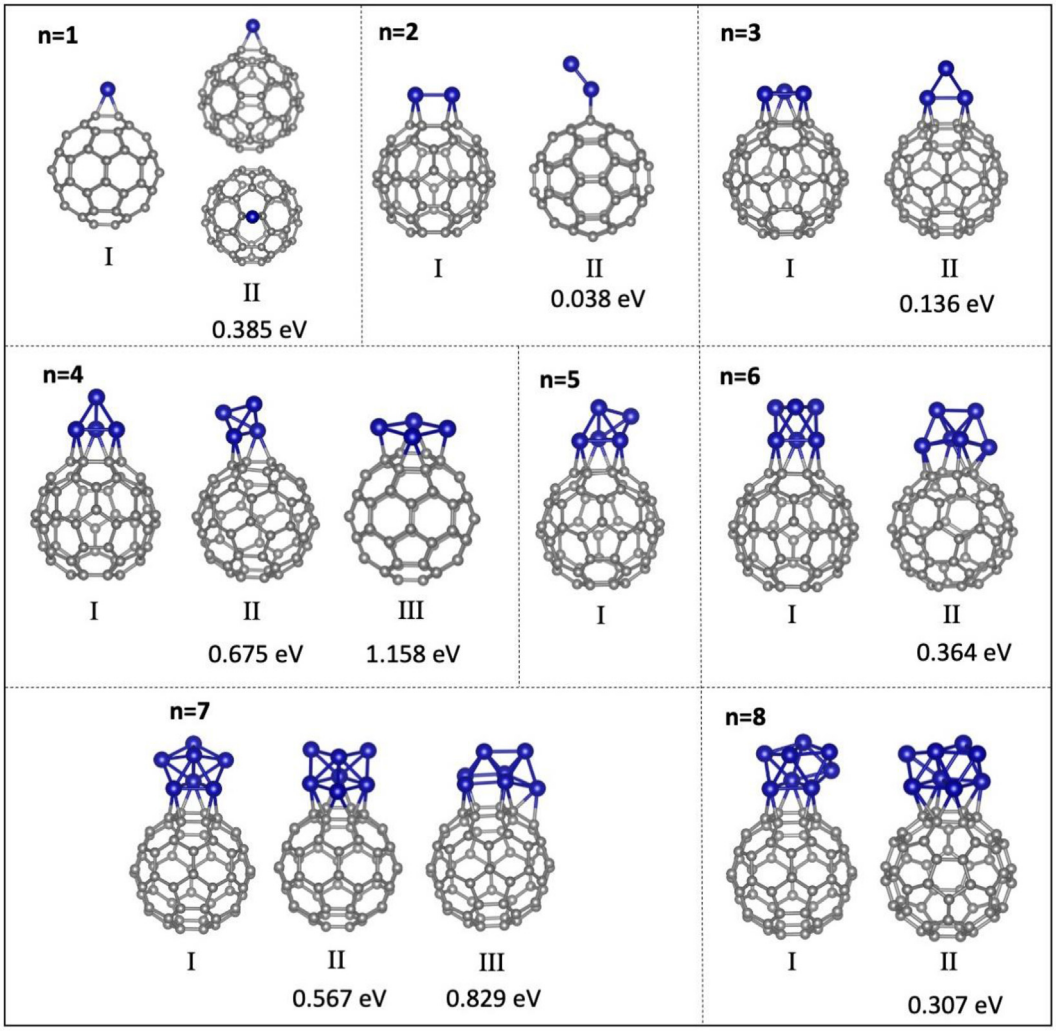

Fig. 1 – Lowest energy structures and isomeric structures of neutral $C_{60}Co_n$ complexes (n = 1–8). The energies of the isomers with respect to the corresponding lowest energy configurations are also given. Grey and blue spheres represent carbon and cobalt atoms, respectively. (For interpretation of the references to colour in this figure legend, the reader is referred to the Web version of this article.)

(see Fig. 1). For the larger clusters, n = 4–8, wetting of the fullerene surface by the Co atoms was also explored. Wetting configurations with four Co atoms in contact with the fullerene were found for n = 4, 6, 7 and 8, and one wetting configuration with five Co atoms in contact with the fullerene was also found for n = 7. As can be observed in Fig. 1, the wetting configurations involve large deformations of Co_n with respect to the free clusters and are between 0.3 eV and 1.2 eV less stable than the corresponding lowest energy structures with three Co atoms in direct contact with the fullerene. These observations are consistent with earlier work showing the clustering of Ti atoms on the surface of the C_{60} fullerene [28]. The lowest energy structures of neutral $C_{60}Co_n$, n = 1–8, are the same as those previously reported for cationic $C_{60}Co_n^+$ complexes [34]. There are just small bond length differences between cationic and neutral complexes, and these differences become smaller as the size of the cobalt cluster increases. For instance, in the charged complex $C_{60}Co^+$ the Co-C bond length increases by 3% compared to the neutral, while for $C_{60}Co_4^+$ the average Co-C bond length increases by 1%. A similar behavior is found for the Co-Co bonds; for $C_{60}Co_2^+$ this bond lengthens by 4% with respect to the neutral, and for $C_{60}Co_4^+$ the average Co-Co bond length increases by 0.5% only.

The adsorption binding energies of the clusters,

$$E_b(Co_n) = E(Co_n) + E(C_{60}) - E(C_{60}Co_n) \quad (1)$$

are given in Table 1. In this equation, the energy E(Co_n) corresponds to the most stable structure of free Co_n, and E($C_{60}Co_n$) corresponds to the lowest energy structure of the complex in Fig. 1. As expected, the adsorption binding energy increases from Co to Co_3. But interestingly, its value is not constant between Co_3 and to Co_8, in spite of the fact that the contact face with C_{60} is formed by three Co atoms in all the cases.

We next consider the process of adding the Co atoms one by one, and the binding energies of each newly added Co atom

$$E_b(n) = E(C_{60}Co_{n-1}) + E(Co) - E(C_{60}Co_n), \quad (2)$$

are plotted in Fig. 2. In this equation $E(C_{60}Co_{n-1})$ and $E(C_{60}Co_n)$ are the total energies of the cobalt-fullerene complexes before and after adding the nth Co atom, and E(Co) is the energy of a free Co atom. $E_b(1)$, that is, the binding energy of the first Co atom adsorbed, whose value is 1.56 eV, measures the Co-fullerene bonding. This bonding arises from the covalent interaction between the Co atom and its two neighbor C atoms. Fig. 3 shows the hybridization between Co and fullerene states, which mainly occurs for spin up states. $E_b(2)$, the energy of the second atom adsorbed, and $E_b(3)$, increase sharply because of the contributions of Co-fullerene and Co-Co bonding. The energies $E_b(n)$ with n = 4–8 reflect the Co-Co bonding. The average value, 4.01 eV, is substantially larger than $E_b(1)$, and this is the reason for the clustering of the Co atoms on the surface of C_{60}. The binding energies $E_b(n)$ are compared in Fig. 2 with the corresponding binding energies for the cationic complexes (the numerical values of the binding energies are given in Table S1 of the Supplementary Information). The most notorious difference is found in the adsorption energy of the first cobalt atom: it is 2.52 eV for the charged complex, and 1.56 eV for the neutral. For further addition of Co atoms, the adsorption energies on neutral and charged substrates are quite similar, with a dip in $C_{60}Co_5$. A minor difference between neutral and charged complexes is that the maximum on the left of the dip occurs at $C_{60}Co_4$ in the neutrals and at $C_{60}Co_3^+$ in the cations.

Table 1 – Adsorption binding energy of Co_n clusters adsorbed on C_{60}.

Co_n	Ads. energy (eV)
Co	1.56
Co_2	2.11
Co_3	3.15
Co_4	3.70
Co_5	3.17
Co_6	2.04
Co_7	2.82
Co_8	2.46

The local redistribution of the electron density when the Co_n cluster is adsorbed on the fullerene

$$\Delta\rho(\vec{r}) = \rho[C_{60}Co_n](\vec{r}) - \rho[C_{60}](\vec{r}) - \rho[Co_n](\vec{r}), \quad (3)$$

gives information on the nature of the cluster-fullerene bonding. To calculate the density redistribution from eq. (3), the free C_{60} and Co_n are placed in the same positions they occupy in $C_{60}Co_n$ and with the same internal geometry. The calculated $\Delta\rho(\vec{r})$ is shown in Fig. 4 for $C_{60}Co_n$ with n = 1–4. The main observation is that the electron redistribution, which reflects the bonding between Co_n and C_{60}, is quite localized in the region of the Co cluster and the closest C atoms. In $C_{60}Co$, the Co atom is in a bridge position between two C atoms, and $\Delta\rho(\vec{r})$ shows an accumulation of electronic charge between the Co atom and those two C atoms which reveals the formation of covalent bonds. This charge displacement produces a charge deficit in the region of the Co atom. A similar picture of formation of covalent bonds occurs for $C_{60}Co_2$, but the charge deficit around the Co atoms is smaller compared to $C_{60}Co$. The density redistribution in $C_{60}Co_2$ shows neither positive nor negative $\Delta\rho$ contours in the region between the two Co atoms. This is clearly visualized in the lateral view of $C_{60}Co_2$ in Fig. 4, and indicates that the Co-Co bond changes little after adsorption of Co_2 on the fullerene. The shape of $\Delta\rho$ becomes increasingly complex in $C_{60}Co_3$ and $C_{60}Co_4$, but reflects the motion of electronic charge to the regions of the Co-C bonds.

Next, we investigate the localization of the electronic charge defect (missing charge) in the cationic complexes $C_{60}Co_n^+$, that is, after the ionization of the neutrals, by calculating

$$\Delta\rho^+(\vec{r}) = \rho[C_{60}Co_n^+](\vec{r}) - \rho[C_{60}Co_n](\vec{r}), \quad (4)$$

with both complexes $C_{60}Co_n^+$ and $C_{60}Co_n$ in the geometry of $C_{60}Co_n^+$. Surfaces of constant value of $\Delta\rho^+(\vec{r})$ are plotted in Fig. 5. Regions in blue and yellow colors correspond to negative and positive values of $\Delta\rho^+(\vec{r})$, respectively, so the electronic deficit after ionization is localized in the blue regions. The blue regions show that the electronic charge lost by ionization comes from the Co atoms mainly [46]. The deficit of electronic charge is evenly distributed between the two Co atoms in $C_{60}Co_2^+$. The first ionization energy of the complexes is displayed in Table 2. The tendency is a decrease of the first ionization energy with n.

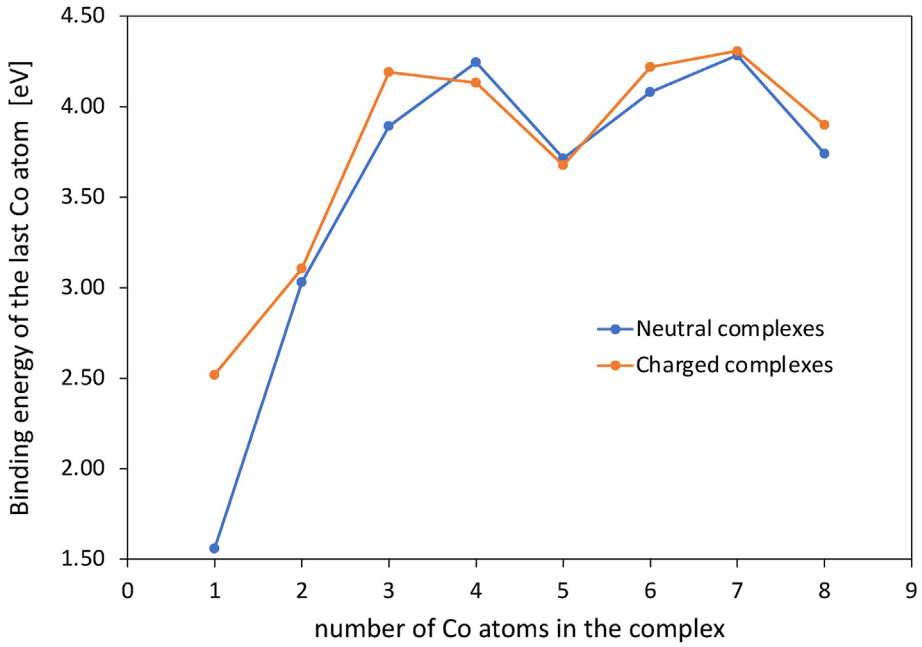

Fig. 2 – Binding energy of the last added Co atom in neutral $C_{60}Co_n$ and cationic $C_{60}Co_n^+$, given in eq. (2).

Molecular and dissociative adsorption of hydrogen

Adsorption of one hydrogen molecule on $C_{60}Co_n$ leads to the structures shown in Fig. 6. Lateral and top views are given in each case. In $C_{60}Co$ to $C_{60}Co_5$ the hydrogen molecule is adsorbed on top of a Co atom in contact with the fullerene. Instead, in $C_{60}Co_6$, $C_{60}Co_7$ and $C_{60}Co_8$ the molecule is adsorbed on one of the Co atoms not in contact with the fullerene. Molecular adsorption does not significantly modify the geometry of the $C_{60}Co_n$ complex. In all cases, the adsorption geometries are very similar to those for the adsorption of H_2 on cationic $C_{60}Co_n^+$ complexes [34], with one exception: in $C_{60}Co_5^+$ the hydrogen molecule is adsorbed on top of a Co atom not in contact with the fullerene, but the

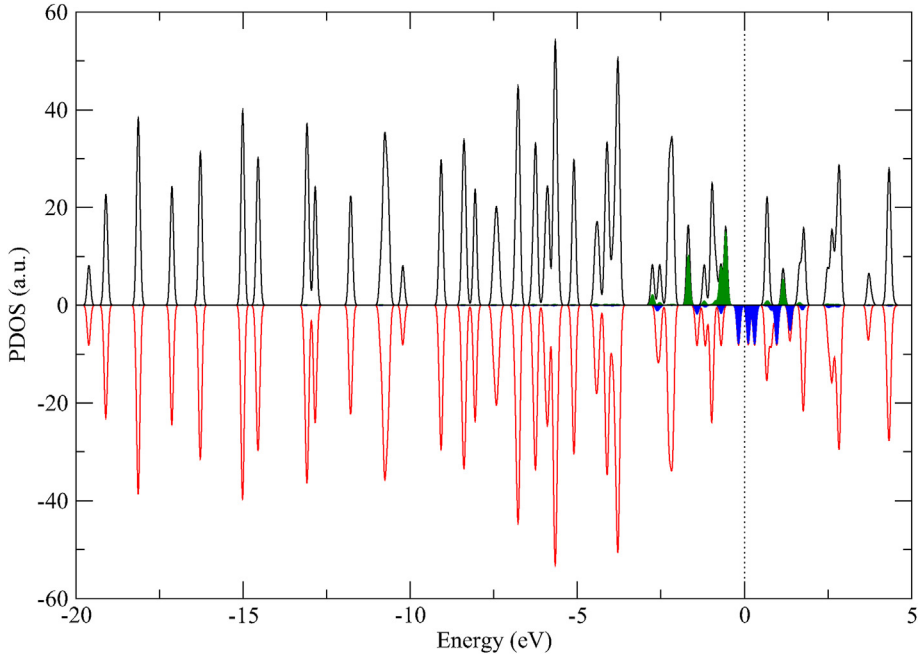

Fig. 3 – Density of electronic states in $C_{60}Co$. Spin up and spin down states are given in black and red color, respectively. The zero energy corresponds to the Fermi energy. Cobalt partial density of states with spin up and down in green and blue color, respectively. (For interpretation of the references to colour in this figure legend, the reader is referred to the Web version of this article.)

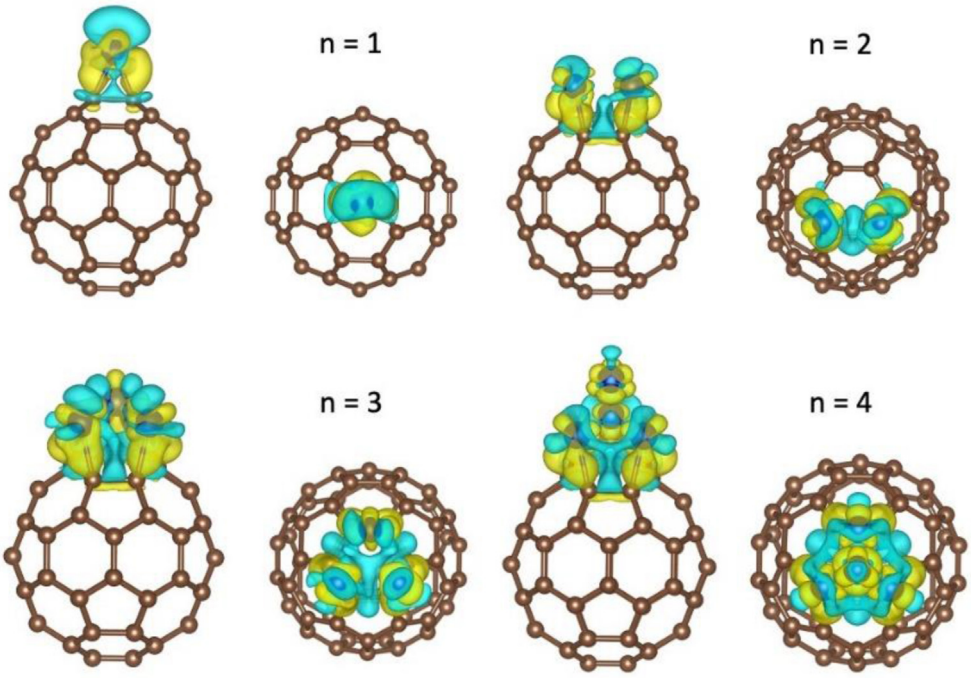

Fig. 4 – Local electron density redistribution $\Delta\rho(\vec{r})$ upon formation of $C_{60}Co_n$ from C_{60} and Co_n for n = 1–4. Lateral and front views are shown in each case. Surfaces of constant $\Delta\rho(\vec{r}) = \pm$ 0.004 e Å^{-3} have been plotted, where the yellow color correspond to positive values of $\Delta\rho(\vec{r})$, that is, regions where the electron density increases with respect to the reference formed by C_{60} and Co_n, and the regions in blue color correspond to negative values of $\Delta\rho(\vec{r})$. (For interpretation of the references to colour in this figure legend, the reader is referred to the Web version of this article.)

molecule is tumbled in such a way that one H atom interacts with one Co atom in contact with the fullerene [34]. Fig. 6 also reports the structures corresponding to dissociative

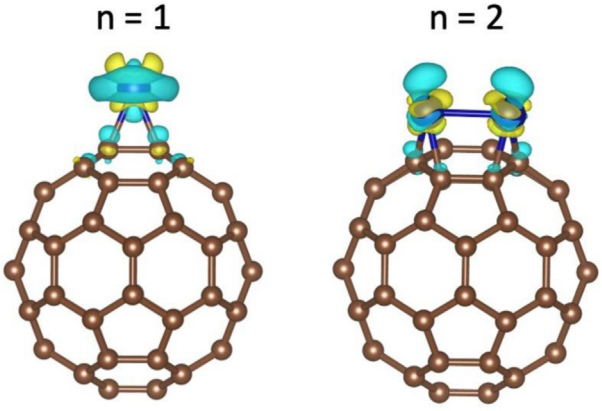

Fig. 5 – Electron density difference $\Delta\rho^+(\vec{r})$ between $C_{60}Co_n^+$ and $C_{60}Co_n$ (both with the geometrical structure of the cation), for n = 1 and 2. Surfaces of constant $\Delta\rho^+(\vec{r}) = \pm$ 0.004 e Å^{-3} are plotted. Blue color regions correspond to negative values of $\Delta\rho^+(\vec{r})$, regions with a deficit of electronic charge in $C_{60}Co_n^+$, and regions in yellow color to positive values of $\Delta\rho^+(\vec{r})$. (For interpretation of the references to colour in this figure legend, the reader is referred to the Web version of this article.)

hydrogen adsorption. The hydrogen atoms occupy bridge positions between neighbor cobalt atoms, just as it occurs in the case of the cationic complexes [34]. An interesting observation is the lack of a dissociative adsorption state either on $C_{60}Co$ and $C_{60}Co^+$. Both clean and hydrogenated Co-fullerene complexes are magnetic. The spin magnetic moments of the clean and hydrogenated neutral $C_{60}Co_n$ and charged $C_{60}Co_n^+$ complexes are reported in Table S2 of the Supplementary Information.

The binding energies for molecular and dissociative adsorption, defined as

$$E_{ads}(H_2) = E[C_{60}Co_n] + E[H_2] - E[H_2@C_{60}Co_n] \quad (5)$$

$$E_{ads}(2H) = E[C_{60}Co_n] + E[H_2] - E[2H@C_{60}Co_n] \quad (6)$$

Table 2 – Ionization energy for $C_{60}Co_n$ n = 1–8, in eV.

n	IE [eV]
1	6.37
2	6.29
3	5.99
4	6.11
5	6.14
6	6.00
7	5.88
8	5.70

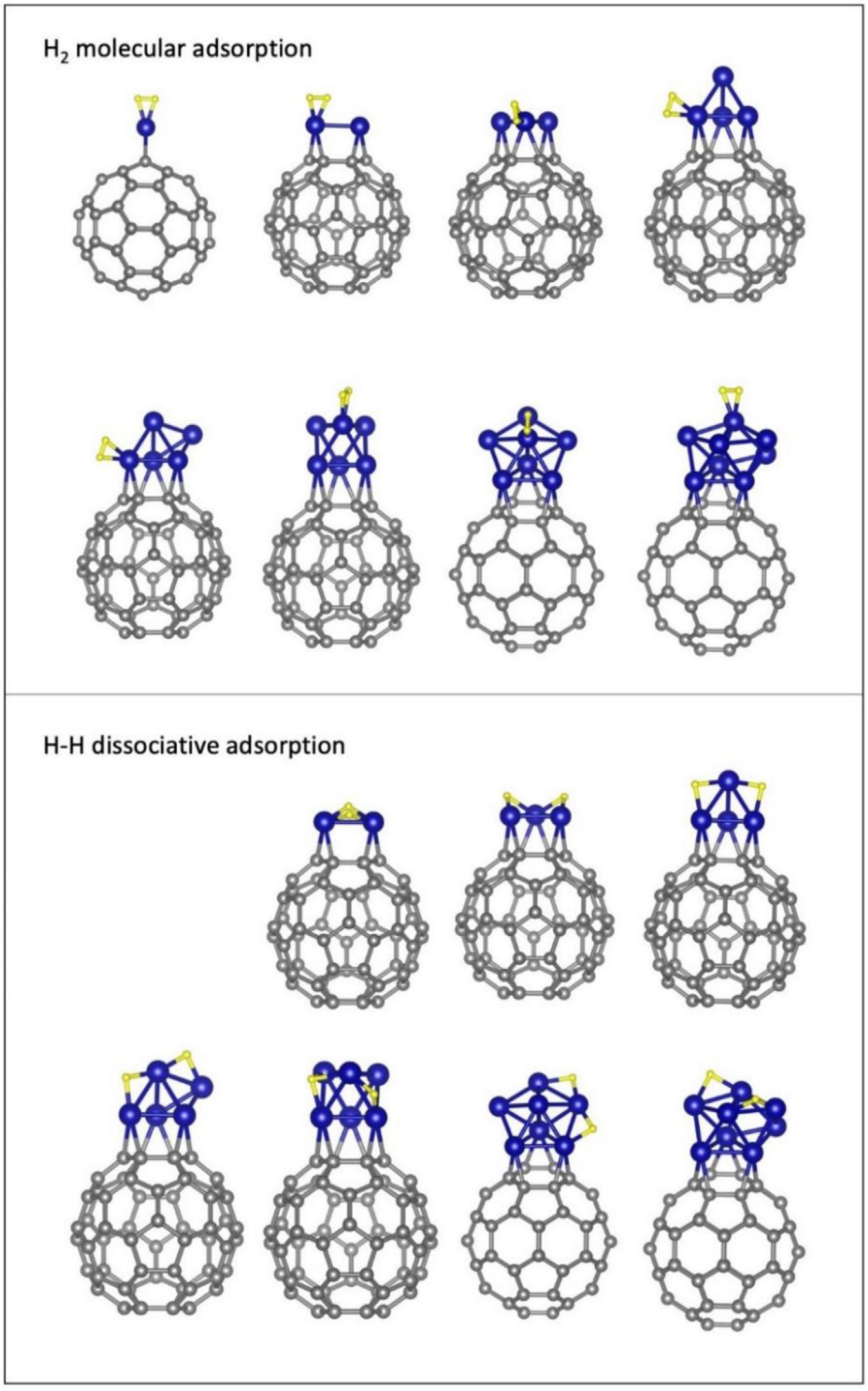

Fig. 6 – Structures corresponding to molecular (H_2) and dissociative (2H) adsorption on neutral $C_{60}Co_n$ complexes, n = 1–8. Grey, blue and yellow spheres represent C, Co and H atoms, respectively. (For interpretation of the references to colour in this figure legend, the reader is referred to the Web version of this article.)

are shown in Fig. 7. The adsorption mode does not depend of the charge state of the complexes: dissociative adsorption (dashed curves) is energetically favored over molecular adsorption (continuous curves) on neutral ($C_{60}Co_n$) and charged ($C_{60}Co_n^+$) complexes. The only exceptions are the near-equal values of the molecular and dissociative adsorption energies on $C_{60}Co_2^+$, and the lack of a dissociated state for n = 1. The behavior of the two curves for molecular adsorption is similar, although the curves cross; that is, the molecular adsorption on neutral clusters is slightly larger than on cationic complexes for some values of n, while for other values of n the opposite occurs. The differences between the

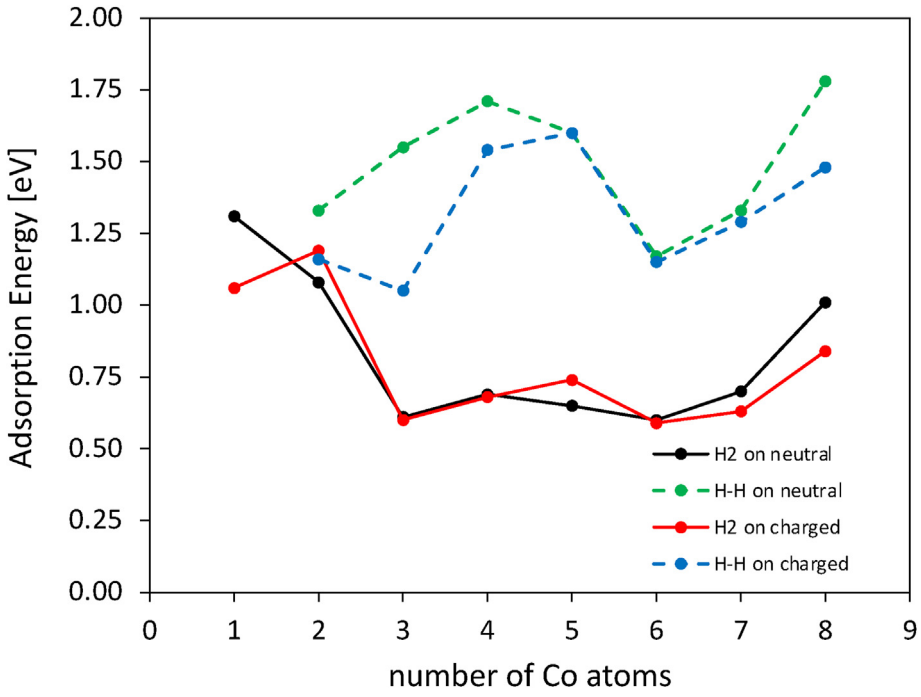

Fig. 7 – Molecular and dissociative hydrogen adsorption energies on $C_{60}Co_n$ and $C_{60}Co_n^+$ complexes. Numerical values are given in Table S3 of the Supplementary Information.

dissociative adsorption energies on neutral and cationic complexes are larger. The noticeable differences in dissociative adsorption energy occur for n = 2, 3, 4, and 8. In those cases, the dissociative adsorption energies on the neutral complexes are clearly larger, in spite of the fact that the dissociative adsorption geometries are rather similar.

It is intriguing that only molecular adsorption is possible for $C_{60}Co$ and $C_{60}Co^+$. Observation of Fig. 6 (and Fig. 4 of the work by Vanbuel et al. [34]) reveals that in the dissociated state the H atoms occupy bridge positions between neighbor Co atoms. This is possible when the Co cluster attached to the fullerene has two or more atoms, but not for a single Co atom. In addition, there is a second interesting contributing effect. Figs. 4 and 5 reveal a deficit of electronic charge in the region of the Co atom in both $C_{60}Co$ and $C_{60}Co^+$; that is, the Co atom is positively charged. Then, following the argument put forward by Niu et al. [47], the Co atom does not have electrons available to be transferred to the antibonding state of the H_2 molecule and dissociation of the molecule does not occur. Instead, the charged Co atom polarizes the charge of the H_2 molecule and binding between H_2 and the Co atom develops due to the charge-dipole interaction.

For n = 2, dissociative adsorption is preferred on neutral $C_{60}Co_2$, and molecular and dissociative adsorption are competitive on cationic $C_{60}Co_2^+$, although the energy of the molecular adsorption state is slightly more stable by 0.03 eV (see Fig. 7). As discussed above, the electron deficit on the Co atoms in the neutral $C_{60}Co_2$ complex is quite small and does not interfere with the tendency of H_2 to dissociate and form covalent H-Co bonds. Instead, Fig. 5 indicates that the positive charge on the Co atoms on $C_{60}Co_2^+$ is substantial, and this effect interferes with the natural tendency of H_2 to dissociate and form covalent H-Co bonds. For this reason, the molecular and dissociative adsorption modes are competitive.

The redistribution of the electron density following molecular adsorption of H_2 on neutral $C_{60}Co_n$ and charged $C_{60}Co_n^+$ complexes can be quantified by $\Delta\rho(\vec{r})$:

$$\Delta\rho^0(\vec{r}) = \rho[H_2@C_{60}Co_n](\vec{r}) - \rho[C_{60}Co_n](\vec{r}) - \rho[H_2](\vec{r}), \quad (7)$$

$$\Delta\rho^+(\vec{r}) = \rho\left[H_2@C_{60}Co_n^+\right](\vec{r}) - \rho\left[C_{60}Co_n^+\right](\vec{r}) - \rho[H_2](\vec{r}), \quad (8)$$

shown in Fig. 8 for n = 1, 2. The electron density redistribution is restricted to the region occupied by the Co atoms and the H_2 molecule and confirms the expected polarization of the molecule. In the case of n = 2 one can appreciate that the molecular adsorption on one of the Co atoms does not affect the Co-Co bonding.

Fig. 8 shows the electron redistribution in the case of dissociated hydrogen (2H) for n = 2, defined

$$\Delta\rho^0(\vec{r}) = \rho[2H@C_{60}Co_2](\vec{r}) - \rho[C_{60}Co_2](\vec{r}) - \rho[2H](\vec{r}), \quad (9)$$

$$\Delta\rho^+(\vec{r}) = \rho\left[2H@C_{60}Co_2^+\right](\vec{r}) - \rho\left[C_{60}Co_2^+\right](\vec{r}) - \rho[2H](\vec{r}). \quad (10)$$

That is, the electron density of the final system minus the densities of the individual isolated fragments, $C_{60}Co_2$ (or $C_{60}Co_2^+$) and two H atoms in the appropriate positions. The electron density increases around the H atoms, at the expense of a loss of charge by the Co atoms; more in the case of the charged complex. This reflects the typical bonding in metallic hydrides, which has also been observed if H_2 dissociates on the surface of free Co clusters [48]. The effect of the C_{60} substrate appears to be minor.

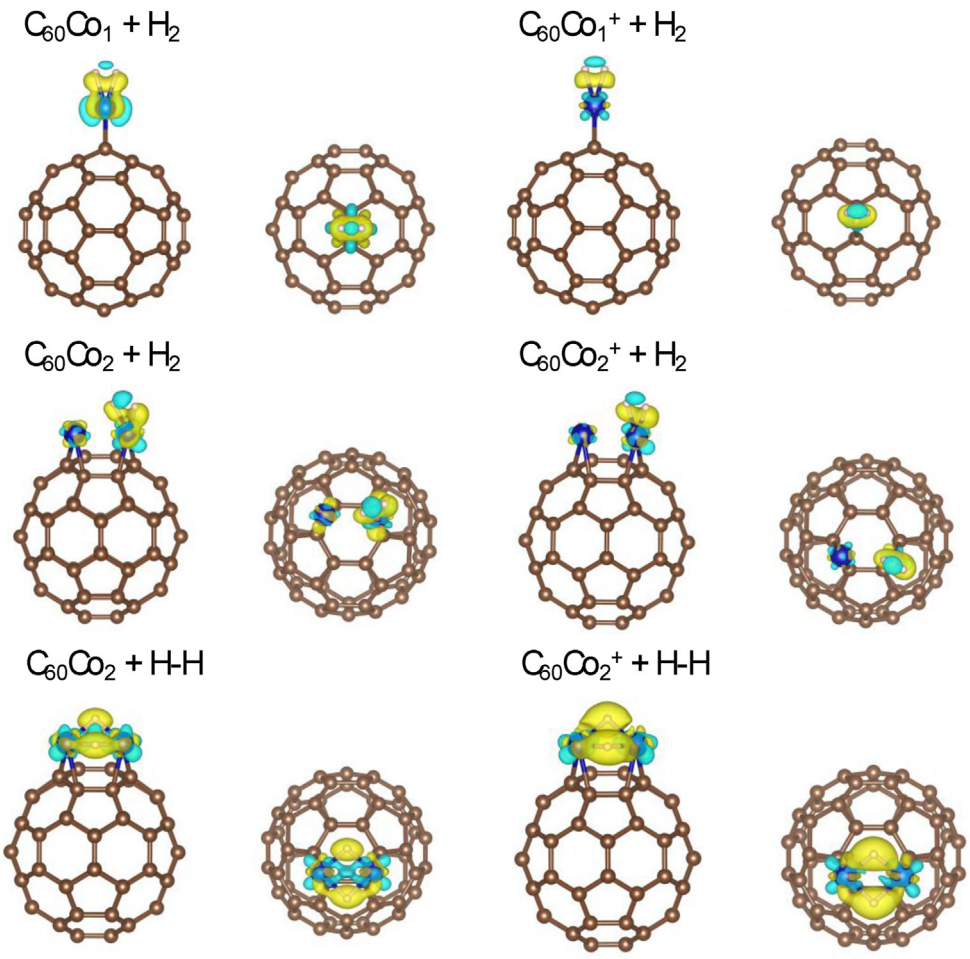

Fig. 8 – Electron density redistribution $\Delta\rho(\vec{r})$ associated to molecular adsorption of H_2 on $C_{60}Co_n$ and $C_{60}Co_n^+$ complexes with n = 1 (upper panels), and 2 (medium panels). The bottom panels show $\Delta\rho(\vec{r})$ for dissociative adsorption (2H) on neutral and charged complexes with n = 2. Surfaces of $\Delta\rho(\vec{r}) = \pm$ 0.01 e Å^{-3} are plotted. Yellow and blue colors correspond to positive and negative values of $\Delta\rho(\vec{r})$ respectively, indicating a local increase or a lowering of the electronic density with respect to the reference. Lateral and top views are shown in each case. (For interpretation of the references to colour in this figure legend, the reader is referred to the Web version of this article.)

To understand the hydrogenation process, not only the energy difference between molecular and dissociative adsorption but also activation barriers are important. The activation barriers for the dissociation of the adsorbed H_2 molecule are shown in Fig. 9 for neutral $C_{60}Co_n$ and charged $C_{60}Co_n^+$ complexes with n = 2–8. There is a substantial variation of the barrier height with the size of the Co cluster, which has been noticed for other metal clusters before [49]. In the charged complexes the dissociation barriers are either low (smaller than 0.1 eV) or intermediate (between 0.1 and near 0.3 eV). The variation of the dissociation barriers with n, and the fact that molecular adsorption is more stable for $C_{60}Co^+$ and $C_{60}Co_2^+$ complexes, was essential in a previous work [34] to explain the experimental desorption rates of H_2 from hydrogenated $C_{60}Co_n^+$ clusters that were formed by reacting H_2 and the $C_{60}Co_n^+$ clusters in a few-collision reaction cell. It was found that desorption of H_2 occurs from the molecular adsorption state, but not from the dissociated state. So, a high activation barrier implies that the system remains for a longer time in the molecular $C_{60}Co_nH_2^+$ state and thus H_2 desorption is more likely. On the other hand, low activation barriers indicate that it is likely that the system may reach the more stable dissociated (2H) state, explaining the low H_2 desorption rates measured in the experiment. In the neutral systems, H_2 dissociation involves energy barriers of 0.2 eV or lower. Since the dissociated state is, in addition, more stable than the molecular state for n ≥ 2 (see Fig. 7) H_2 dissociation in neutral $C_{60}Co_n$ is expected to be easy.

Saturation with hydrogen

Adsorption of additional hydrogen has been investigated in two representative complexes, $C_{60}Co$ and $C_{60}Co_6$. In this process we only consider hydrogen adsorbed on the Co or Co_6 parts of the complex. The adsorption energies corresponding to the sequential addition of individual H_2 molecules

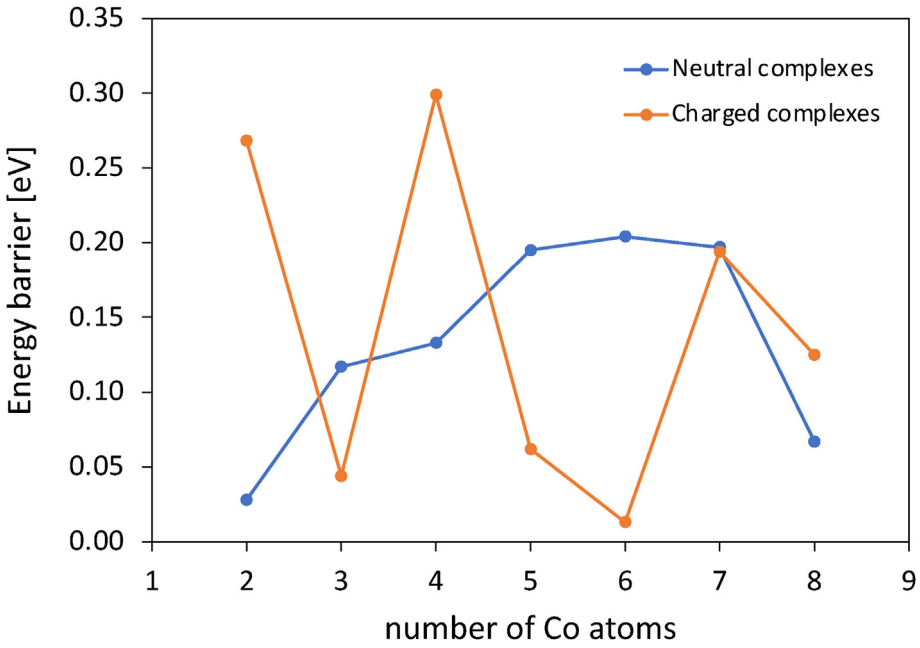

Fig. 9 – Calculated barrier heights for H_2 dissociation on neutral $C_{60}Co_n$ and charged $C_{60}Co_n^+$ complexes with n = 2–8.

$$E_{ads}(H_2) = E\left[(H_2)_x@C_{60}Co_n\right] + E\left[H_2\right] - E\left[(H_2)_{x+1}@C_{60}Co_n\right] \quad (11)$$

are given in Fig. 10. It was noticed in Section Molecular and dissociative adsorption of hydrogen above that $C_{60}Co$ is exceptional in the $C_{60}Co_n$ group, because a preference for molecular adsorption occurs for the first H_2 molecule. $C_{60}Co$ can adsorb two more H_2 units, also in molecular form. The adsorption energy decreases for the second and the third molecule. The fourth molecule is not bound, that is, the corresponding value of $E_{ads}(H_2)$ is negative (the process is endothermic). The adsorbed H_2 molecules avoid each other, as shown for the case of three H_2 molecules in Fig. S1.

The first three adsorbed H_2 units dissociate on $C_{60}Co_6$, and the H atoms occupy bridge positions on the lateral edges of the Co_6 octahedron. The adsorption energies are larger than 1 eV. The structure of the Co cluster suffers severe distortions, and two Co-Co bonds break up for two and three adsorbed H_2 molecules. Those are bonds between Co atoms of the triangular face in contact with the fullerene. The case of three dissociated molecules ($6H@C_{60}Co_6$) is shown in Fig. 11(a), where the broken-bond Co-Co distances are both equal to 3.23 Å, much larger than the original Co-Co bond lengths in bare $Co_{60}Co_6$, which vary between 2.31 and 2.38 Å. The two broken-bond Co-Co distances in the case of two dissociated molecules are even larger, 3.42 and 3.37 Å.

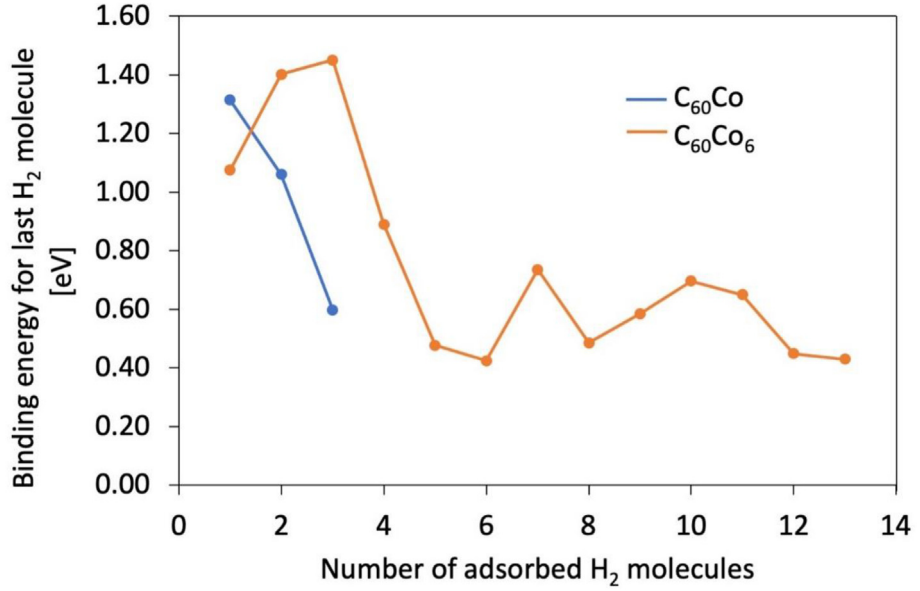

Fig. 10 – Adsorption energies of the first, second, etc., H_2 molecules on $C_{60}Co$ and $C_{60}Co_6$.

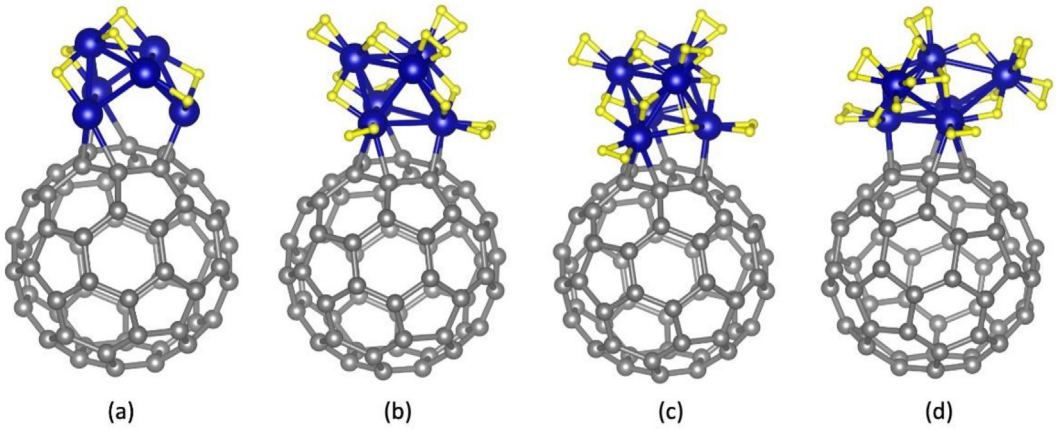

Fig. 11 – Calculated structures of: (a) $(H_2)_3@C_{60}Co_6$, with the three molecules dissociated; (b) $(H_2)_9@C_{60}Co_6$, with the three molecules dissociated and six non-dissociated; (c) $(H_2)_{10}@C_{60}Co_6$, with the four molecules dissociated and six non-dissociated; (d) $(H_2)_{13}@C_{60}Co_6$, with four molecules dissociated and nine non-dissociated. Grey, blue and yellow spheres represent C, Co and H atoms, respectively. (For interpretation of the references to colour in this figure legend, the reader is referred to the Web version of this article.)

As more H_2 molecules are added, from the fourth to the ninth molecule, each one of these is adsorbed in molecular form on a different Co atom, while the previously adsorbed molecules do not alter their positions. The adsorption energies are below 1 eV. The structure of $(H_2)_9@C_{60}Co_6$, given in Fig. 11(b), shows that the Co_6 cluster recovers much of its original octahedral form, although distorted. The bond lengths between the Co atoms of the triangular face in contact with the fullerene are 2.75 Å, 2.44 Å, and 2.39 Å. After the six Co atoms are exhausted, the tenth adsorbed molecule dissociates and the H atoms take positions on top of two triangular faces of the Co octahedron (see Fig. 11 (c)). The Co-Co bond lengths in the face in contact with the fullerene are 2.81 Å, 2.69 Å, and 2.49 Å. The Co_6 octahedron is, in fact, a bit swollen, presumably to increase the adsorption surface. The adsorption energy of the tenth molecule does not reach the large values obtained for the first three dissociated molecules. Finally, the system admits three more, non-dissociated, H_2 molecules, which adopt adsorption positions on the three Co atoms which are not in contact with the fullerene. The adsorption of the thirteenth molecule leads to a change in the structure of the Co cluster. As shown in Fig. 11(d), one Co-Co bond of the upper triangle of the octahedron breaks up and the new structure can be viewed as formed by two Co_4 tetrahedrons sharing an edge. Attempts to add more molecules were unsuccessful, since the process becomes endothermic. In summary, $C_{60}Co_6$ is able to adsorb up to thirteen hydrogen molecules, four of these dissociated and nine in non-dissociated. Interestingly, the adsorption energies, shown in Fig. 10, are in all cases larger than 0.4 eV.

Table 3 – Minimum temperature to desorb one H_2 molecule from $(H_2)_x@C_{60}Co$ and $(H_2)_x@C_{60}Co_6$.

$(H_2)_x@C_{60}Co$		$(H_2)_x@C_{60}Co_6$	
X	T (K)	x	T (K)
1	878	1	729
2	720	2	932
3	434	3	962
		4	615
		5	359
		6	327
		7	520
		8	365
		9	426
		10	495
		11	466
		12	342
		13	330

The structure of the curve giving the binding energy of the last molecule in $(H_2)_x@C_{60}Co_6$ has local maxima for a number of adsorbed H_2 molecules $x_m = 3$, 7, and 10. This is reminiscent of the well-known magic numbers of clusters [50–52], and indicates that $(H_2)_3@C_{60}Co_6$, $(H_2)_7@C_{60}Co_6$ and $(H_2)_{10}@C_{60}Co_6$ are more stable than neighbor clusters with a number of H_2 molecules different from x_m. These binding energies (or evaporation energies) control the hydrogen desorption temperatures from the $(H_2)_x@C_{60}Co_6$ complexes. The minimum temperatures to evaporate one H_2 molecule from $(H_2)_x@C_{60}Co$ and $(H_2)_x@C_{60}Co_6$ are given in Table 3, and details of the calculation appear in the Supplementary Information. However, those are not the temperatures required to desorb all the molecules of the complex. We take as an example the saturated complex $(H_2)_{13}@C_{60}Co_6$. By heating an ensemble of $(H_2)_{13}@C_{60}Co_6$ complexes in an oven, most complexes will evaporate a hydrogen molecule at a temperature about 330K. To desorb the second and the third molecules, the temperature has to rise up to 342K and 466K, respectively. Evaporation of the fourth molecule requires rising again the temperature, up to 495K, but at this point each complex evaporates not only one, but three molecules. To desorb more molecules, the temperature has to rise up to 520K, and at this temperature each complex evaporates three molecules. Following the argument, evaporation of the tenth molecule needs a temperature of 615K. Finally, the last three molecules of each complex desorb at 962K; substantially higher, in fact, than

the temperature of 330K needed to desorb the first molecule of the complex. This is, evidently, a typical finite size effect.

Summary and conclusions

The molecular and dissociative adsorption of H_2 on neutral $C_{60}Co_n$ complexes with n = 1–8 has been investigated using density functional theory and dispersion interaction corrections. A comparison with the case of adsorption on cationic $C_{60}Co_n^+$ complexes has been made. The Co atoms form compact clusters on the surface of C_{60}. In all cases from $C_{60}Co_3$ to $C_{60}Co_8$, three Co atoms (forming a triangular face of the cluster) make the contact between the Co cluster and the fullerene. In spite of this fact, the binding energy between the Co cluster and the fullerene shows some variation with the cluster size. When $C_{60}Co_n$ is ionized, the electronic charge deficit becomes localized mainly in the cobalt cluster. Dissociative chemisorption of H_2 is energetically more stable than molecular adsorption on $C_{60}Co_n$. The only exception occurs for $C_{60}Co$, and the reason is that a single adsorbed Co atom cannot form separate covalent bonds with the two H atoms because its bonding capacity is in part exhausted by the Co-fullerene interaction. On the other hand, for n = 2 or higher, each H atom binds to two nearest-neighbor Co atoms in a bridge position between those two atoms. The molecular and dissociative adsorption features on cationic $C_{60}Co_n^+$ and neutral $C_{60}Co_n$ complexes are rather similar, but some differences can be noticed. Molecular H_2 adsorption and dissociative adsorption on $C_{60}Co_2^+$ are competitive; in fact, molecular adsorption is slightly more stable. This is a result of the cationic nature of the complex. The positive charge (deficit of electrons) is localized on the Co dimer, and this makes difficult the transfer of electronic charge to the antibonding electronic orbital of H_2, making the adsorbed molecular state competitive. A second difference is that the dissociative adsorption energies on some of the cationic $C_{60}Co_n^+$ complexes are substantially smaller than the dissociative adsorption energies on the corresponding (same n) neutral complexes by amounts varying between 0.2 and 0.5 eV. The activation barriers for H_2 dissociation strongly depend on size n and also on the charge of the complex. These barriers help to interpret the adsorption state (molecular or dissociated) of experimentally produced hydrogenated $C_{60}Co_n^+$ complexes. Saturation with hydrogen has been studied in two cases. $C_{60}Co$ can adsorb three H_2 units in molecular form, and $C_{60}Co_6$ can adsorb up to thirteen H_2 units, four dissociated and nine in molecular form. Due to the current interest on carbon nanostructured materials as candidates to build hydrogen storage devices, this work helps to clarify the physicochemical processes taking place when hydrogen is adsorbed on metal-doped carbon nanostructures.

Declaration of competing interest

The authors declare that they have no known competing financial interests or personal relationships that could have appeared to influence the work reported in this paper.

Acknowledgments

Work supported by Junta de Castilla y León (Grant VA021G18), Ministerio de Ciencia e Innovación of Spain (Project PID2019-104924RB-I00) and University of Valladolid (GIR Nanostructure Physics). Estefanía German acknowledges a postdoctoral contract with the University of Valladolid. The authors thankfully acknowledge the computer resources at Calendula (SCAYLE) and the technical support provided by Barcelona Supercomputing Center (FI-2019-3-0029); and also the facilities provided by Centro de Proceso de Datos-Parque Científico (University of Valladolid).

Appendix A. Supplementary data

Supplementary data to this article can be found online at https://doi.org/10.1016/j.ijhydene.2021.03.179.

REFERENCES

[1] Schlapbach L, Zuttel A. Hydrogen-storage materials for mobile applications. Nature 2001;414:353–8.
[2] Jena P. Materials for hydrogen storage: past, present, and future. J Phys Chem Lett 2011;2:206–11.
[3] Wang L, Yang RT. New sorbents for hydrogen storage by hydrogen spillover - a review. Energy Environ Sci 2008;1:268–79.
[4] Dillon AC, Jones KM, Bekkedahl TA, Klang CH, Bethune DS, Heben MJ. Storage of hydrogen in single-walled carbon nanotubes. Nature 1997;386:377–9.
[5] Liu C, Fan YY, Liu M, Cong HT, Cheng HM, Dresselhaus MS. Hydrogen storage in single-walled carbon nanotubes at room temperature. Science 1999;286:1127–9.
[6] Mananghaya MR. Hydrogen adsorption of nitrogen-doped nanotubes functionalized with scandium. Int J Hydrogen Energy 2015;40:9352–8.
[7] Mananghaya MR, Santos GN, Yu D. Hydrogen adsorption of Ti-decorated boron nitride nanotube: a density functional based tight binding molecular dynamics study. Adsorption 2018;24:683–90.
[8] Mananghaya MR, Yu D, Santos GN. Hydrogen adsorption on boron nitride nanotubes functionalized with transition metals. Int J Hydrogen Energy 2016;41:13531–9.
[9] Gao Y, Wu XJ, Zeng XC. Designs of fullerene-based frameworks for hydrogen storage. J Mater Chem A 2014;2:5910–4.
[10] Ayub K. Transportation of hydrogen atom and molecule through $X_{12}Y_{12}$ nano-cages. Int J Hydrogen Energy 2017;42:11439–51.
[11] Tachikawa H, Iyama T. Mechanism of hydrogen storage in the graphene nanoflake–lithium–H_2 system. J Phys Chem C 2019;123:8709–16.
[12] Bakhshi F, Farhadian N. Co-doped graphene sheets as a novel adsorbent for hydrogen storage: DFT and DFT-D3 correction dispersion study. Int J Hydrogen Energy 2018;43:8355–64.
[13] Huang Jianyu, Liang Yeru, Dong Hanwu, Hu Hang, Yu Peifeng, Peng Lin, Zheng Mingtao, Xiao Yong, Liu Yingliang. Revealing contribution of pore size to high hydrogen storage capacity. Int J Hydrogen Energy 2018;43:18077–82.

[14] Wróbel-Iwaniec I, Díez N, Gryglewicz Grazyna. Chitosan-based highly activated carbons for hydrogen storage. Int J Hydrogen Energy 2015;40:5788–96.
[15] Yushin G, Dash R, Jagiello J, Fischer JE, Gogotsi Y. Carbide-derived carbons: effect of pore size on hydrogen uptake and heat of adsorption. Adv Funct Mater 2006;16:2288–93.
[16] Patchkovskii S, Tse JS, Yurchenko SN, Zhechkov L, Heine T, Seifert G. Graphene nanostructures as tunable storage media for molecular hydrogen. Proc Natl Acad Sci USA 2005;102:10439–44.
[17] Cabria I, López MJ, Alonso JA. Simulation of the hydrogen storage in nanoporous carbons with different pore shapes. Int J Hydrogen Energy 2011;36:10748–59.
[18] Harmas R, Palm M, Russina M, Kurig H, Grzimek V, Hark E, Koppel M, Tallo I, Paalo M, Oll O, Embs J, Lust E. Transport of H_2 confined in carbide-derived carbons with different pores and sizes. Carbon 2019;155:122–8.
[19] Rosi NL, Eckert J, Eddaoudi M, Vodak DT, Kim J, O'Keeffe M, Yaghi OM. Hydrogen storage in microporous metal-organic frameworks. Science 2003;300:1127–9.
[20] Côté AP, Benin AI, Ockwig NW, O'Keeffe M, Matzger AJ, Yaghi OM. Porous, crystalline, covalent organic frameworks. Science 2005;310:1166–70.
[21] Mao WL, Koh CA, Sloan ED. Clathrate hydrates under pressure. Phys Today 2007;60(10):42–7.
[22] Arellano JS, Molina LM, Rubio A, Alonso JA. Density functional study of adsorption of molecular hydrogen on graphene layers. J Chem Phys 2000;112:8114–9.
[23] Arellano JS, Molina LM, Rubio A, López MJ, Alonso JA. Interaction of molecular and atomic hydrogen with (5,5) and (6,6) single-wall carbon nanotubes. J Chem Phys 2002;117:2281–8.
[24] López MJ, Cabria I, Alonso JA. Simulated porosity and electronic structure of nanoporous carbons. J Chem Phys 2011;135:104706.
[25] Contescu CI, van Benthem K, Li S, Bonifacio CS, Pennycook SJ, Jena P, Gallego NC. Single Pd atoms in activated carbon fibers and their contribution to hydrogen storage. Carbon 2011;49:4050–8.
[26] Contescu CI, Brown CM, Liu Y, Bhat VV, Gallego NC. Detection of hydrogen spillover in palladium-modified activated carbon fibers during hydrogen adsorption. J Phys Chem C 2009;113:5886–90.
[27] Zhao Y, Kim YK, Dillon AC, Heben MJ, Zhang SB. Hydrogen storage in novel organometallic buckyballs. Phys Rev Lett 2005;94:155504.
[28] Sun Q, Wang Q, Jena P, Kawazoe Y. Clustering of Ti on a C_{60} surface and its effect on hydrogen storage. J Am Chem Soc 2005;127:14582–3.
[29] Sun Q, Jena P, Wang Q, Marquez M. First-principles study of hydrogen storage on $Li_{12}C_{60}$. J Am Chem Soc 2006 2006;128:9741–5.
[30] Yoon M, Yang S, Hicke C, Wang E, Geohegan D, Zhang Z. Calcium as the superior coating metal in functionalization of carbon fullerenes for high-capacity hydrogen storage. Phys Rev Lett 2008;100:206806.
[31] Ren H, Cui C, Li X, Liu Y. A DFT study of the hydrogen storage potentials and properties of Na- and Li-doped fullerenes. Int J Hydrogen Energy 2017;42:312–21.
[32] Kuganathan N, Chroneos A. Hydrogen adsorption on Ru-encapsulated, -doped and -supported surfaces of C_{60}. Surfaces 2020;3:408–22.
[33] Kaiser A, Renzler M, Kranabetter L, Schwärzler M, Parajuli R, Echt O, Scheier P. On enhanced hydrogen adsorption on alkali (cesium) doped C_{60} and effects of the quantum nature of the H_2 molecule on physisorption energies. Int J Hydrogen Energy 2017;42:3078–86.
[34] Vanbuel J, Germán E, Libeert G, Veys K, Moens J, Alonso JA, López MJ, Janssens E. Reactivity of cobalt-fullerene complexes towards deuterium. ChemPhysChem 2020;21:1012–8.
[35] Giannozzi P, Baroni S, Bonini N, Calandra M, Car R, Cavazzoni C, Ceresoli D, Chiarotti GL, Cococcioni M, Dabo I, et al. Quantum Espresso: a modular and open-source software project for quantum simulations of materials. J Phys Condens Matter 2009;21:395502.
[36] www.quantum-espresso.org/pseudopotentials.
[37] Perdew JP, Burke K, Ernzerhof M. Generalized gradient approximation made simple. Phys Rev Lett 1996;77:3865–8.
[38] Hammer B, Hansen LB, Nørskov JK. Improved adsorption energetics within density-functional theory using revised Perdew-Burke-Ernzerhof functionals. Phys Rev B 1999;59:7413–21.
[39] Grimme S, Antony J, Ehrlich S, Krieg H. A consistent and accurate ab initio parametrization of density functional dispersion correction (DFT-D) for the 94 elements H-Pu. J Chem Phys 2010;132:154104.
[40] Makov G, Payne MC. Periodic boundary conditions in ab initio calculations. Phys Rev B 1995;51:4014–22.
[41] Henkelman G, Uberuaga BP, Jónsson H. A climbing image nudged elastic band method for finding saddle points and minimum energy paths. J Chem Phys 1995;113:9901–4.
[42] Sheppard D, Terrell R, Henkelman G. Optimization methods for finding minimum energy paths. J Chem Phys 2008;128:134106.
[43] Marín P, Alonso JA, Germán E, López MJ. Nanoalloys of metals which do not form bulk alloys: the case of Ag–Co. J Phys Chem A 2020;124:6468–77.
[44] Datta S, Kabir M, Ganguly S, Sanyal B, Saha-Dasgupta T, Mookerjee A. Structure, bonding, and magnetism of cobalt clusters from first-principles calculations. Phys Rev B 2007;70:165403.
[45] Ma QM, Xie Z, Wang J, Liu Y, Li YC. Structures, stabilities and magnetic properties of small Co clusters. Phys Lett A 2006;358:289–96.
[46] Robledo M, Aguirre NF, Díaz-Tendero S, Martín F, Alcamí M. Bonding in exohedral metal-fullerene cationic complexes. RSC Adv 2014;4:53010–20.
[47] Niu J, Rao BK, Jena P, Manninen M. Interaction of H_2 and He with metal atoms, clusters, and ions. Phys Rev B 1995;51:4475–84.
[48] García-Díez K, Fernández-Fernández J, Alonso JA, López MJ. Theoretical study of the adsorption of hydrogen on cobalt clusters. Phys Chem Chem Phys 2018;20:21163–76.
[49] Cabria I, López MJ, Fraile S, Alonso JA. Adsorption and dissociation of molecular hydrogen on palladium clusters supported on graphene. J Phys Chem C 2012;116:21179–89.
[50] Alonso JA. Structure and properties of atomic nanoclusters. 2nd ed. London: Imperial College Press; 2012.
[51] Echt O, Sattler K, Recknagel E. Magic numbers for sphere packings: experimental verification in free xenon clusters. Phys Rev Lett 1981;47:1121–4.
[52] de Heer WA. The physics of simple metal clusters: experimental aspects and simple models. Rev Mod Phys 1993;65:611–76.